Sliding-Mode-Based Direct Power Control of Dual-Active-Bridge DC-DC Converters

Kerui Li, Yun Yang, Siew-Chong Tan, Ron Shu-Yuen Hui
Department of Electrical and Electronic Engineering
The University of Hong Kong
Hong Kong
Email:krli@eee.hku.hk; cacaloto@hku.hk, sctan@eee.hku.hk, ronhui@eee.hku.hk

***Abstract*- For very good reasons, there are significant interests in applying nonlinear control to dual-active-bridge (DAB) DC-DC converters. This paper presents a sliding-mode-based direct power controller for the power flow control of DAB converters. The proposed scheme exploits both the advantages of sliding-mode control and direct power control, thus leading to accurate reference tracking, fast dynamic response, large-signal stability, and high robustness against line and load disturbance. The design procedure of this controller is provided. Both simulation and experimental results are provided to verify the performances. Compared to the existing control schemes, the proposed controller exhibits better performance. The line and load regulation are 0.25% and 0.4% of the nominal output voltage, respectively.**

Keywords-dual active bridge converters, direct power control, sliding mode control

I. Introduction

Dual-active-bridge (DAB) converters [1] are widely used in DC bus management applications that require bidirectional DC-DC power conversions [2]–[4]. An important function of the DAB converter is to maintain a stable DC bus voltage against load and other external disturbance [5]. There are many reported research works on its control, which aimed at achieving accurate reference voltage tracking, fast output voltage dynamic response and large signal stability. Earlier works are based on the use of the small-signal model of the DAB converter for the design of its (linear) controller [6]. The main drawback of applying linear controllers to DAB converters is that in the event that the operation point (load, input voltage, etc.) deviates, its control performance will be severely degraded. This spurred the work on using direct power control [1] along with the small-signal model of DAB converter, to improve the output voltage large-signal performance (as compared to linear controllers) [7]. To strengthen the robustness property of the DAB converter against the line and load disturbances, the input-voltage and output-current feedforward control schemes have been respectively introduced to the linear controller [8] and [9]. In [10], a nonlinear control scheme utilizing both the input voltage and output current feedforward control is proposed to combine the merits of robustness against both line and load disturbances. The development trend indicates that the introduction of nonlinearity into the control improves the performance, but it lacks a systematical method to manage and design the nonlinear stages. Consequently, the attention is now focused on developing feasible nonlinear control schemes for the DAB converters.

Among the nonlinear control schemes, the sliding mode (SM) control is found to be one of the most effective for power converters because of its high robustness against disturbance and fast programmable response [11]–[15]. Previous attempts on using SM control in DAB converter are reported in [16] and [17]. In these works, the controller involves full-order SM control schemes, which are designed to regulate the output voltage/current directly. Unfortunately, such full-order SM controllers are computationally exhaustive, but produce limited improvement in performance as compared to reduced-order equivalent SM controllers (which are much simpler to implement). More importantly, the direct output voltage/current control contradicts the mechanism of DAB converter: the output current/voltage is regulated by the power flow, while the power flow is directly controlled by the phase-shift ratio, indicating that a "translator" is required to bridge the SM control and the DAB converter. The direct power control scheme can be an ideal option in power "translation". The control law of the SM control can emulate the desired power after the calculation of output voltage/current error, while the direct power control scheme translates the power into the phase-shift ratio. Following this idea, an SM-based direct power control (DPC) scheme is proposed in this paper. Here, an equivalent reduced-order SM controller is used to process the output error and emulate the desired power, of which the DPC scheme decodes the emulated power into the corresponding phase-ratio ratio. The proposed scheme exploits the advantages of SM control and DPC, thus leading to accurate reference tracking, fast dynamic response, large-signal stability, and high robustness against line and load disturbances.

II. Analysis of the Conventional DPC

Fig. 1 shows the topology of a typical bidirectional power flow DAB DC-DC converter, which comprises a full bridge voltage-source inverters, a full bridge voltage-source active rectifier and a 1:*n* transformer in series with the inductance *L*.

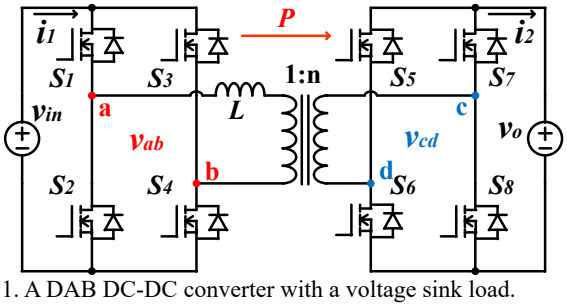

Fig. 1. A DAB DC-DC converter with a voltage sink load.

The gate driving signals and key waveforms of the DAB converter with phase-shift modulation are plotted in Fig. 2. Here, the voltages v_{ab} and v_{cd} are controlled by the driving signals with a phase-shift ratio of $D \in [-0.5, 0.5]$.

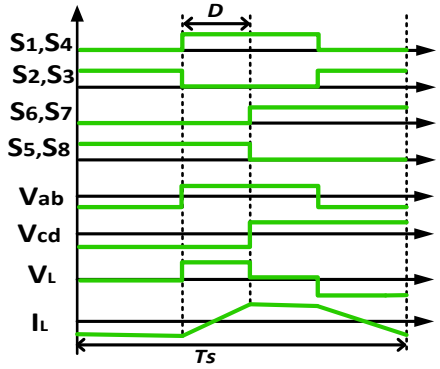

Fig. 2. Key waveforms of the DAB DC-DC converter under phase-shift modulation.

Assuming ideal lossless conversion, the transmission power P can be calculated using

$$P=\begin{cases}\dfrac{v_{in}v_o D(1-D)}{2nLf_s}, P>0\\ \dfrac{v_{in}v_o D(D+1)}{2nLf_s}, P\le 0\end{cases} \tag{1}$$

where f_s is the switching frequency of the converter and L is the leakage inductance of the transformer [1]. The maximum transmission power $P_{\max}$ and the minimum transmission power $P_{\min}$ are obtained at D=0.5 and D=−0.5, respectively, where

$$-\frac{v_{in}v_o}{8nLf_s}=P(D=-0.5)=P_{\min}\le P\le P_{\max}=P(D=0.5)=\frac{v_{in}v_o}{8nLf_s}. \tag{2}$$

Besides, the phase-shift ratio D can be derived based on (1) as

$$D=\begin{cases}\dfrac{1}{2}-\sqrt{\dfrac{1}{4}-\dfrac{2nLf_sP}{v_{in}v_o}}, if\ \dfrac{v_{in}v_o}{8nLf_s}\ge P>0\\ -\dfrac{1}{2}+\sqrt{\dfrac{1}{4}+\dfrac{2nLf_sP}{v_{in}v_o}}, if\ -\dfrac{v_{in}v_o}{8nLf_s}\le P\le 0\end{cases}. \tag{3}$$

Apparently, the transmission power P can be directly regulated by varying D. As a result, fast dynamic power tracking of the DAB converter within the range of available transmission power described by (2) can be achieved.

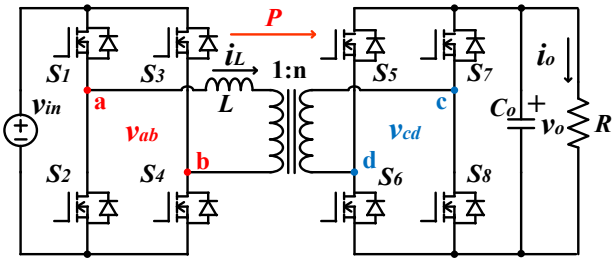

Fig. 3. DAB DC-DC converter with resistive load.

III. Design Procedures of the Proposed SM-Based DPC

To simplify the analysis without losing generality, the proposed SM-based DPC is designed for a unidirectional power flow DAB converter, as shown in Fig. 3. Here, the

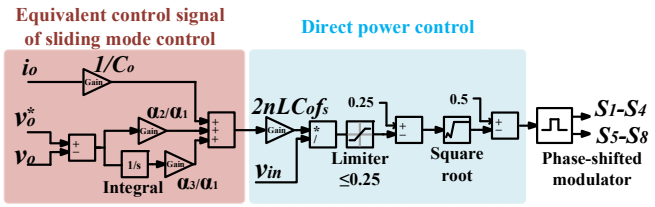

Fig.4. Schematic diagram of the proposed SM based direct power controller for the DAB DC-DC converter.

output voltage v_o across the filtering capacitor C_o and the output resistor R_o is relatively constant at steady state. The relationship corresponding to power P and energy E_{Co} of the capacitor is

$$\frac{dE_{C_o}(t)}{dt}=\frac{d\,\frac{1}{2}C_o v_o(t)^2}{dt}=P(t)-v_o(t)i_o(t). \tag{4}$$

By substituting (1) into (4), we have

$$\frac{dv_o(t)}{dt}=\frac{v_{in}D(1-D)}{2nLC_of_s}-\frac{i_o(t)}{C_o}. \tag{5}$$

Then, the state variables of the sliding surface are selected. The error of the output voltage and its integral term is used. A second-order integral term of the output voltage error is further used to eliminate the steady-state error of the equivalent SM control. The state variables for SM-based DPC are chosen as

$$\boldsymbol{x}=[x_1(t),x_2(t),x_3(t)]^T=\left[v_o^*-v_o(t),\int_0^t(v_o^*-v_o(\tau))d\tau,\int_0^t x_2(\tau)d\tau\right]^T, \tag{6}$$

where v_o^* is the output voltage reference. The sliding surface is chosen as

$$S(t)=[\alpha_1,\alpha_2,\alpha_3][x_1(t),x_2(t),x_3(t)]^T, \tag{7}$$

where coefficients are chosen as α_1>0, α_2>0, and α_3>0 to ensure that Routh-Hurwitz stability criterion is satisfied for the designated sliding surface. The control law for the sliding mode is designed as

$$D=\begin{cases}0.5, if\ S(t)>0\\ 0, if\ S(t)<0\end{cases}. \tag{8}$$

Besides, to satisfy the existence conditions, the following inequality must be complied, i.e.,

$$\lim_{S(t)\to 0}S(t)\frac{dS(t)}{dt}<0$$

$$\Rightarrow$$

$$\begin{cases}\dfrac{dS(t)}{dt}=\alpha_1\left(\dfrac{i_o}{C_o}-\dfrac{v_{in}}{8nLC_of_s}\right)+ & \\ \alpha_2(v_o^*-v_o(t))+\alpha_3\int(v_o^*-v_o(t))dt<0, & if\ S(t)\to 0^+\\ \dfrac{dS(t)}{dt}=\alpha_1\left(\dfrac{i_o}{C_o}\right)+\alpha_2(v_o^*-v_o(t))+ & \\ \alpha_3\int(v_o^*-v_o(t))dt>0, & if\ S(t)\to 0^-\end{cases}$$

$$\Rightarrow$$

$$0<8nLf_si_o+8nLC_of_s\left(\frac{\alpha_2}{\alpha_1}\right)(v_o^*-v_o(t))+8nLC_of_s\left(\frac{\alpha_3}{\alpha_1}\right)\int(v_o^*-v_o(t))dt<v_{in} \tag{9}$$

Next, the equivalent control law can be derived based on $dS(t)/dt=0$, which results in the phase-shift ratio D of

$$D=\frac{1}{2}-\sqrt{\frac{1}{4}-\frac{2nLC_o f_s P_{SM}}{v_{in}}}. \quad (10)$$

where

$$P_{SM}=\frac{i_o}{C_o}+\frac{\alpha_2}{\alpha_1}(v_o^*-v_o(t))+\frac{\alpha_3}{\alpha_1}\int(v_o^*-v_o(t))dt\cdot \quad (11)$$

The equivalent control law (10) comprises two components: (11) the equivalent control scheme of the SM control (highlighted in red) and (10) DPC scheme (highlighted in blue). The equivalent control of the SM control processes the output voltage error and derives a corresponding virtual power P_{SM}. Afterwards, the DPC scheme translates P_{SM} into phase-shift ratio D. The control block diagram of the proposed SM-based DPC is depicted in Fig. 4. The dynamics of the controlled variables can be determined by setting appropriate values for coefficients α_1, α_2, and α_3. Equation (12) shows that the dynamic response is second order and that the coefficients can be selected via Ackerman's formula [14].

$$\frac{\partial^2 S(t)}{\partial t^2}=0 \Rightarrow \frac{\partial^2 x_1(t)}{\partial t^2}+\frac{\alpha_2}{\alpha_1}\frac{dx_1(t)}{dt}+\frac{\alpha_3}{\alpha_1}x_1(t)=0. \quad (12)$$

The dynamics are designed for critical damping second order response and therefore the coefficients are selected as

$$\frac{\alpha_2}{\alpha_1}=4\pi f_{BW}, \frac{\alpha_3}{\alpha_1}=4\pi^2 f_{BW}{}^2, \quad (13)$$

where f_{BW} is the desired bandwidth of the closed-loop system.

IV. Comparative Study in Simulation

A comparative study of the performance of the proposed control scheme and that of conventional control schemes reported in [7]-[9] is conducted in simulation for a 300 W DAB converter with the following parameters: n = 5, L = 5 μH, C_o = 220 μF, v_{in}=40 V, v_o = 200 V, and f_s = 100 kHz. The control parameters are: α_2/α_1=500 and α_3/α_1=6250. All the control schemes, including the proposed control scheme, use the sensors for monitoring the input voltage, the output voltage, and the output current. For fairness of comparison, the control parameters for all the control schemes are tuned to have the same start-up dynamic performance, as shown in Fig. 5(a).

Obviously, the proposed SM-based DPC can regulate the Fig. 5(b) and 5(c) show respectively the waveforms of the DAB converter under the different control schemes for step load change from full load (320 W) to ¼ load (64 W) and a step input voltage change from 40 V to 48 V. Clearly, the proposed SM-based DPC can regulate the output voltage with a lower overshoot and a shorter settling time. The control schemes reported in [7] and [8] uses the control law of PI controller as the phase-shift ratio for phase-shift modulation. The linearity of the PI controller is not suitable for the nonlinear plant like DAB converters. What's more, the mechanism of the DAB converter is to use power to regulate the output voltage. The nonlinear relationship of the power and phase-shift adversely affects the performance of

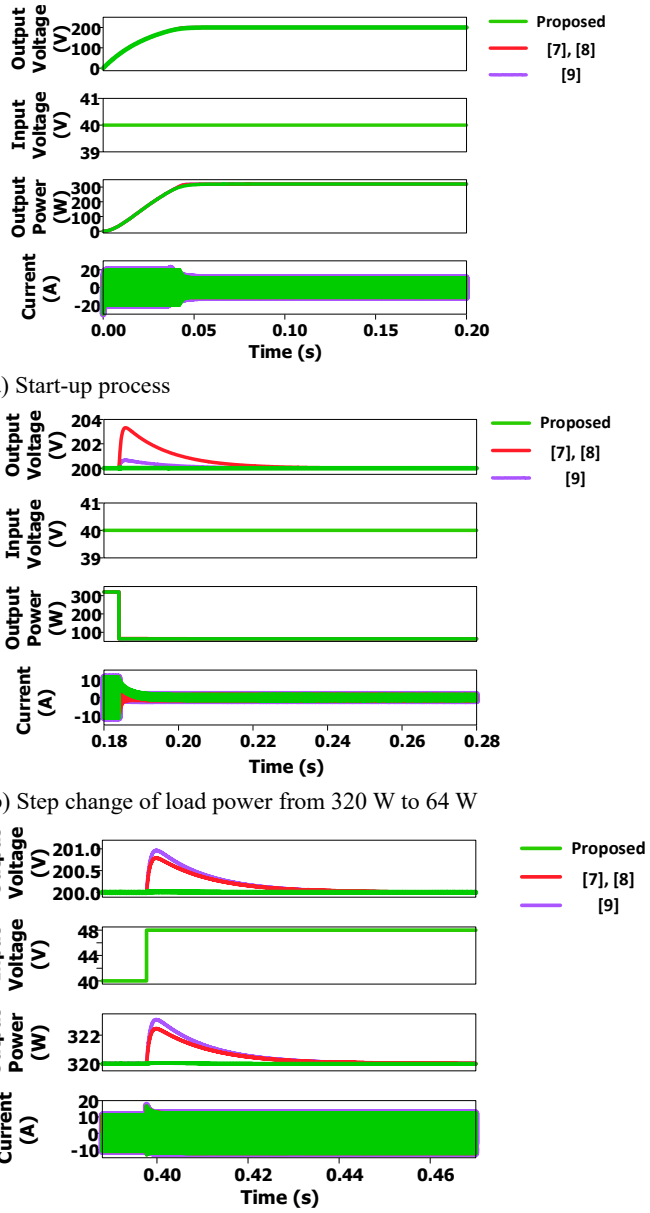

(a) Start-up process

(b) Step change of load power from 320 W to 64 W

(c) Step change of input voltage from 40 V to 48 V

Fig. 5. Comparative simulation results of the DAB converter with different control schemes. (a) Output voltage response of the start-up process; (b) output voltage response of load steps; (c) ouput voltage response of input voltage steps.

the linear PI controller of the control schemes from [7] and [8]. In contrast, the proposed scheme not only uses nonlinear controller but uses a DPC as a translator. In this way, the proposed controller follows the physical mechanism of the DAB converter and obtain the precise phase-shift ratio and overcome the nonlinearity of the converter. This explains why the proposed scheme has better dynamic responses in line and load responses again disturbances. The control scheme from [9] uses DPC scheme to introduce input voltage and design a feedforward path to enhance the dynamic performance. Here, the DPC behaves as a translator and this is why the dynamic responses using the control scheme from [9] are very similar to the responses of the proposed one. However, the control scheme in [9] uses the typical PI controller but the proposed scheme uses the SM controller. The superiority of the SM controller in handling large-signal disturbance results in the proposed scheme

having slightly faster responses and lower overshoots. In all, the use of the DPC scheme can enhance the dynamic response performance, because using the DPC scheme can follow the physical operating mechanism of the DAB converter. Besides, the use of SM control over linear PI control combining with DPC scheme can further spurs the performance as the SM control has high robustness against disturbance and fast programmable response.

V. Experimental Results

A proof-of-concept prototype of the DAB converter is built with identical specifications (output voltage level and power level as that used in simulation). The corresponding components of the prototype are listed in Table I. The control scheme is implemented using a TMS320F28335 microcontroller. The *S* domain parameters of the controller are converted to *Z* domain using Tustin Z transform. Due to the relatively high switching frequency (100 kHz), the converted parameters of the controller are identical to the original ones. As a result, the parameters used in simulation can be directly applied in the experiment. The code of control block diagram of the proposed SM-based DPC scheme, as shown in Fig. 4, is directly generated by PSIM and compiled by Code Composer Studio.

Table I.
Component List of the Prototype

Part	Value	Part Number
MOSFET S_1~S_4		IPB200N15N3
SiC MOSFETs S_5~S_8		C3M0280090D
Gate Driver		ADuM3223*4
Co	114.7 μF	110 μF E-caps and 4.7 μF film caps
Transformer	10:50	EPCOS ETD59 core and Litz wire
Inductance *L*	5.27 μF	Air core inductor with Litz wire
Sensors		AMC 1100*3 (Two for voltage sensing and one for current sensing)
Microcontroller		TMS320F28335

The steady-state waveforms of the converter with closed-loop control are shown in Fig. 6. The transmitted power is 324 W; the phase-shift ratio is approximately 0.29 while the theoretical ratio is calculated as approximately 0.28. The output voltage is 200.45 V while the required output voltage is 200 V. Fig. 7 shows the curves of the output voltage and output power of the DAB converter at different loads. The output voltage varies from 199.75 V to 200.55 V with an output power variation from 69 W to 324 W, resulting in a 0.4% output voltage error in load regulation. Fig. 8 shows the curve of output voltage and power of the DAB converter under the proposed control scheme at vaious input voltages, in which the output voltage varies from 200.38 V to 200.55 V, leading to a maximum 0.25% voltage error.

Fig. 9 shows the dynamic response waveforms (v_{cd}, v_{ab}, i_L and v_o) of the DAB converter operating with load steps from 69 W to 324 W. The output voltage has a small overshoot during the dynamic response and resume to the nominal voltage value afterwards. It is observed that the output voltage has a 3 V overshoot, equaling 1.5% of the nominal output voltage. The settling time is 40 ms. The zoom-in waveforms before and after load steps show that the phase-shift ratio between the waveform of v_{cd} and v_{ab} is increased after the step changes, and the peak-to-peak value of the transmitter current i_L is also increased. Next, a load step change from 324 W to 69 W is performed and the results are shown in Fig. 10. The output voltage has a small undershoot during the dynamic response and resume to the nominal value afterwards. The undershoot is 5 V (equaling 2.5% of the nominal output voltage) and the settling time is 60 ms. The zoom-in waveforms before and after load step show that phase-shift ratio as well as the the peak-to-peak value of the inductor current i_L decreases after load step change. The start-up dynamic with 324 W load is shown in Fig. 11, where no overshoot is observed in the output voltage.

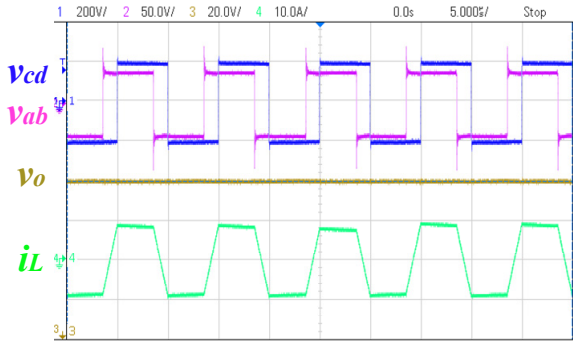

Fig. 6. Steady-state waveforms of the converter. CH1: v_{cd}=200V /div; CH2: v_{ab}=50V/div; CH3: v_o=10V/div; CH4: i_L=10A/div; Time: 5 μs/div.

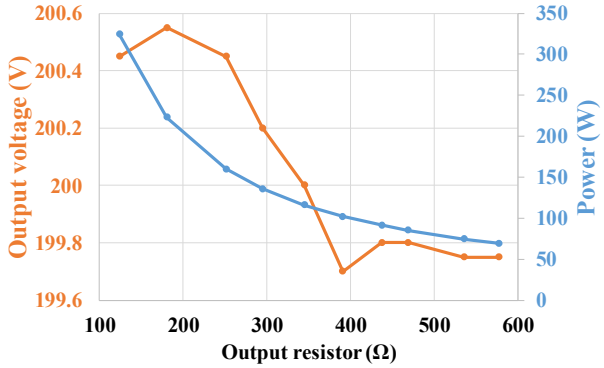

Fig. 7. Measured output voltage and output power of the DAB converter under the proposed control scheme at different loads.

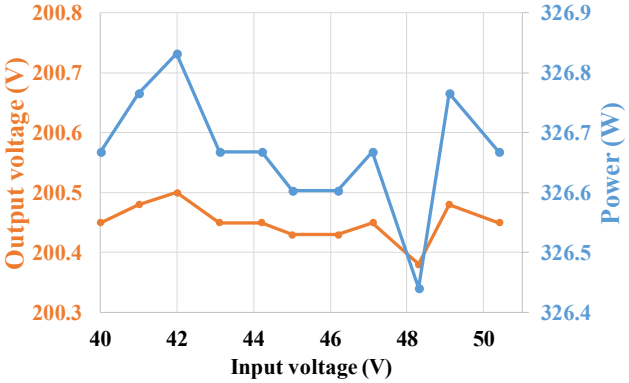

Fig. 8. Measured output voltage and power of the DAB converter under the proposed control scheme at different input voltage.

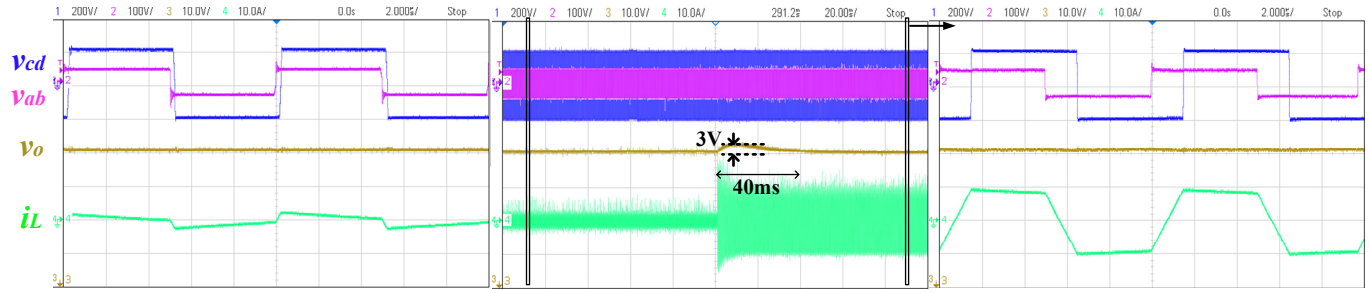

Fig. 9. The dynamic response when load changed from 64 W to 324 W and the corresponding steady-state waveforms.

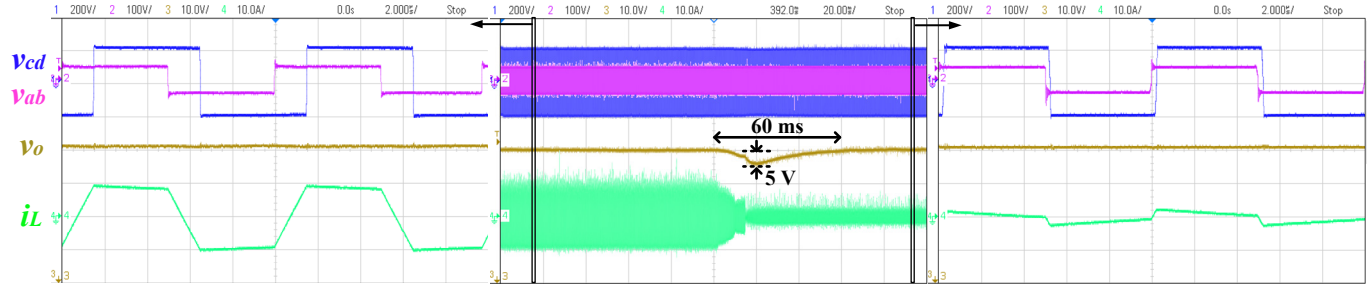

Fig. 10. The dynamic response when load changed from 324 W to 64 W and the corresponding steady-state waveforms.

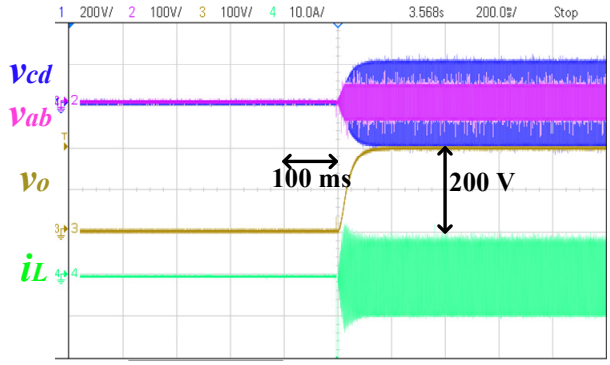

Fig. 11. The dynamic response of startup operation of the DAB converter with the proposed SM-based DPC control scheme.

V. Conclusions

A sliding mode (SM)-based direct power control (DPC) scheme is proposed for the DAB converters. The design procedure and equations are elaborated. The proposed scheme has been verified in simulation and experiment. Simulation results show that the DAB converter using the proposed SM-based DPC can achieve the lowest output voltage overshoot in the case of a load step and input voltage step change, as compared with those using existing control schemes. Experimental results with the proposed control show that the maximum steady-state error of the output voltage within the operation load range and input voltage range are 0.4% and 0.25% of the nominal output voltage, respectively. A 2.5% undershoot of the nominal output voltage is observed when the load steps from ¼ load to full load, while a 1.5% overshoot of nominal output voltage is observed, when the load steps from full load to ¼ load.

References

[1] R. W. A. A. De Doncker, D. M. Divan, and M. H. Kheraluwala, "A three-phase soft-switched high-power-density DC/DC converter for high-power applications," *IEEE Trans. Ind. Appl.*, vol. 27, no. 1, pp. 63-73, Jan/Feb 1991.

[2] M. N. Kheraluwala, R. W. Gascoigne, D. M. Divan, and E. D. Baumann, "Performance characterization of a high-power dual active bridge DC-to-DC converter," *IEEE Trans. Ind. Appl.*, vol. 28, no. 6, pp. 1294-1301, Nov/Dec 1992.

[3] H. Bai and C. Mi, "Eliminate reactive power and increase system efficiency of isolated bidirectional dual-active-bridge DC–DC converters using novel dual-phase-shift control," *IEEE Trans. Power Electron.*, vol. 23, no. 6, pp. 2905-2914, Nov. 2008.

[4] F. Krismer and J. W. Kolar, "Efficiency-optimized high-current dual active bridge converter for automotive applications," *IEEE Trans. Ind. Electron.*, vol. 59, no. 7, pp. 2745-2760, July 2012

[5] B. Zhao, Q. Song, W. Liu, and Y. Sun, "Overview of dual-active-bridge isolated bidirectional DC–DC converter for high-frequency-link power-conversion System," *IEEE Trans. Ind. Electron.*, vol. 29, no. 8, pp. 4091-4106, Aug. 2014.

[6] H. Qin and J. W. Kimball, "Generalized average modeling of dual active bridge DC–DC converter," *IEEE Trans. Power Electron.*, vol. 27, no. 4, pp. 2078-2084, April 2012.

[7] H. Bai, C. Mi, C. Wang, and S. Gargies, "The dynamic model and hybrid phase-shift control of a dual-active-bridge converter", *Proc. 34th Annu. Conf. IEEE Ind. Electron.*, pp. 2840-2845, 2008.

[8] H. Bai, Z. Nie, and C. Mi, "Experimental comparison of traditional phase-shift dual-phase-shift and model-based control of isolated bidirectional DC–DC converters", *IEEE Trans. Power Electron.*, vol. 25, no. 6, pp. 1444-1449, Jun. 2010.

[9] D. Segaran, D. G. Holmes, B. P. McGrath, "Enhanced load step response for a bidirectional dc–dc converter", *IEEE Trans. Power Electron.*, vol. 28, no. 1, pp. 371-379, Jan. 2013.

[10] W. Song, N. Hou, and M. Wu, "Virtual direct power control Scheme of dual active bridge DC–DC converters for fast dynamic response," *IEEE Trans. Power Electron*, vol. 33, no. 2, pp. 1750-1759, Feb. 2018.

[11] R. Venkataramanan, A. Šabanović, and S. Ćuk, "Sliding mode control of DC-to-DC converters," in *Proceedings of IEEE Conf. Ind. Electron., Control and Instrum.*, 1985, pp. 251−258.

[12] H. Sira-Ramirez and M. Ilic, "A geometric approach to the feedback control of switch mode DC-to-DC power supplies," *IEEE Tran. Circuits Syst.*, vol. 35, no. 10, pp. 1291-1298, Oct. 1988.

[13] P. Mattavelli, L. Rossetto, G. Spiazzi, and P. Tenti, "General-purpose sliding-mode controller for DC/DC converter applications," *Proc. IEEE Power Electron. Spec. Conf. - PESC '93*, pp. 609–615, 1993.

[14] L. Martmez-Salamero, J. Calvente, R. Giral, A. Poveda, and E. Fossas, "Analysis of a bidirectional coupled-inductor cuk converter operating in sliding mode," *IEEE Trans. Circuits Syst. I Fundam. Theory Appl.*, vol. 45, no. 4, pp. 355–363, 1998.

[15] S.C. Tan, Y. M. Lai, and C. K. Tse., "Sliding mode control of switching power converters: techniques and implementation", CRC Press, 2011.

[16] Y.Jeung, I. Choi, and D. Lee, "Robust voltage control of dual active bridge DC-DC converters using sliding mode control," *Proc. 2016 IEEE 8th International Power Electronics and Motion Control Conference (IPEMC-ECCE Asia)*, Hefei, pp. 629-634, 2016

[17] M. J. Carrizosa , A. Benchaib , P. Alou, and G. Damm "DC transformer for DC/DC connection in HVDC network", *Proc. 15th Eur. Conf. Power Electron. Appl.*, pp.1 -10 20